

Vertical Cavity Self-Emitting Laser Diode (Mena et al. Model)

VCSEL

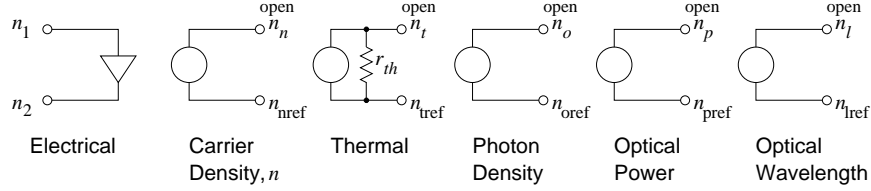


Figure 1: Vertical Cavity Self-Emitting Laser Diode (Mena et al. Model). The terminals labeled open should be connected to opens or very large resistors in a circuit. The reference terminals should be specified as local reference terminals, see the command .REF, e.g. use .REF n_{nref} in the netlist.

fREEDA Form: VCSEL:(instance name) n_1 n_2 n_n n_{nref} n_t n_{tref} n_o n_{oref} n_p n_{pref} n_l n_{lref} (parameter list)

n_1 is the electrical anode terminal

n_2 is the electrical cathode terminal

n_n is the carrier density terminal

n_{nref} is the carrier reference terminal

n_t is the thermal terminal

n_{tref} is the thermal reference terminal

n_o is the photon density terminal

n_{oref} is the photon density reference terminal

n_p is the optical power terminal

n_{pref} is the optical reference terminal

n_l is the wavelength terminal

n_{lref} is the wavelength reference terminal

parameter list see table for parameter list

Note that n_n , n_o , n_p , n_l must be connected to open circuits in the circuit as zero"current" is the solution of an internal equation. The n_t must also be connected to open as the thermal resistance, r_{th} , is included in the model. If r_{th} is open (or a very large value) then this terminal can be connected to a thermal circuit.

The quantities available by printing the voltage at the terminals are as follows (with n_{nref} , n_{oref} , n_{tref} , n_{pref} , and n_{lref} identified as local reference terminals using the .REF command).

“voltage” at terminal n_1 is electrical voltage

“voltage” at terminal n_2 is electrical voltage

“voltage” at terminal n_n is the carrier density

“voltage” at terminal n_t is the temperature in centigrade

“voltage” at terminal n_o is the photon density

“voltage” at terminal n_p is the optical power

“voltage” at terminal n_l is the optical wavelength

Parameter Table

Table 1: Parameters for the VCSEL Laser Diode Model

Parameters	Description	Values	Units
η_i	Injection Efficiency	1	-
β	Spontaneous Emission Coupling Coefficient	1e-6	-
τ_n	Carrier Recombination Lifetime	5e-9	s
k	Output coupling efficiency	2.6e-8	W
g_0	Gain Coefficient	1.6e4	s^{-1}
n_0	Carrier Transparency number	1.94e7	-
τ_p	Photon Lifetime	2.28e-12	s
a_0	1st temperature coefficient of the offset current	1.246e-3	A
a_0	2nd temperature coefficient of the offset current	-2.545e-5	A/K
a_1	3rd temperature coefficient of the offset current	2.908e-7	A/K ²
a_0	4th temperature coefficient of the offset current	-2.531e-10	A/K ³
a_1	5th temperature coefficient of the offset current	1.022e-12	A/K ⁴
ρ	Refractive index change	2.4e-9	-
n	Refractive Index	3.5	-
λ_0	Wavelength	863e-9	m
R_{th}	Thermal Impedance	2.6e3	$^{\circ}\text{C}/\text{W}$
τ_{th}	Thermal time constant	1e-6	s
T_0	Ambient Temperature	20	$^{\circ}\text{C}$

Description

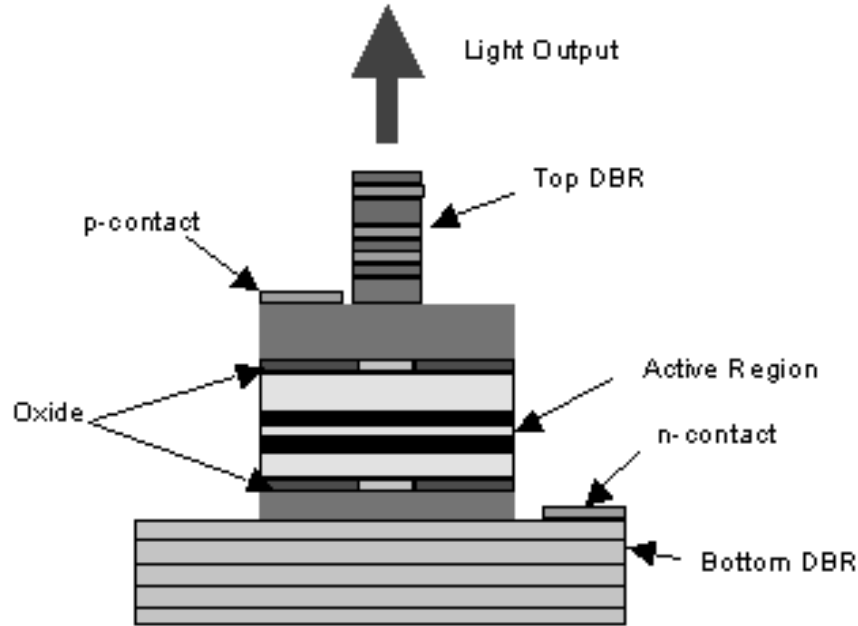


Figure 2: VCSEL Structure laser. After [24].

Vertical-Cavity Surface-Emitting Lasers (VCSEL's) possess a single-longitudinal-mode of operation and a circular output beam. Also their planar structure, where the optical cavity is formed along the device's growth direction as shown in Fig. 2, results in many important advantages such as compatibility with on-wafer probing, and one and two-dimensional (1-D and 2-D) integration of VCSEL arrays. The laser diode analyzed here is an 863 nm bottom-emitting VCSEL with a 16 mm diameter, as described in [22]. The laser diode model is based on the simple thermal VCSEL model developed by Mena *et.al.* [23]. It is a semi-empirical model based on the standard laser rate equations and a thermally dependent empirical offset current. The following sections describe in detail the governing equations of the model and its implementation in FREEDA. The work is described in References [1] and [2].

Analysis

One of the most recognized limitations of a VCSEL's performance is its thermal behavior. Due to the large electrical resistance introduced by the Distributed Bragg Reflector (DBR's) [23] and their poor heat dissipation characteristics, typical VCSEL's undergo relatively severe heating and consequently can exhibit strong thermally dependent behavior. That is why the effects of self heating on the output characteristics of VCSEL's are very significant. For example, thermal lensing can yield considerable differences between cw (continuous wave) and pulsed operation, as well as altering the emission profile of the laser's optical modes. However, the most important effect is exhibited in the device's static LI (light versus current) characteristics. First, as with edge-emitters, VCSEL's exhibit temperature-dependent threshold current. Also, because the active-region temperature increases severely with the injection current, cw operation is limited by a sharp roll-over in the output power [25].

Clearly, for any VCSEL model to be effective for the design of optoelectronic applications, the model

should capture thermal effects, in particular the temperature-dependent threshold current and output power roll-over. Also, the model must be able to simulate both static and dynamic modulation of the laser. To meet the above criteria, the model should be based on temperature dependent rate equations. The strong thermal dependence of VCSEL's can be attributed to a number of mechanisms [23] such as Auger recombination and optical losses, however, the most important effects during static, or cw, operation are due to the temperature-dependent gain and carrier leakage out of the active region. For simplicity, the model in [23] ignores the temperature-dependence of the gain and the carrier leakage is taken into account by introducing a thermally dependent empirical offset current into the model equations.

The above threshold static LI characteristics of the VCSEL can be modeled using $P_o = \eta(T)(I - I_{th}(N, T))$, where P_o is the optical output power, $\eta(T)$ is the temperature dependent differential slope efficiency, I is the injection current, and $I_{th}(N, T)$ is the threshold current as a function of the carrier number N and the active region temperature T . Assuming that the temperature dependence of the differential slope efficiency is minimal, and neglecting the effect of spatial hole burning [23], the output power expression becomes:

$$P_o = \eta(I - I_{th}(T)) \quad (1)$$

where $I_{th}(T)$ can be expressed as a constant value I_{tho} plus an empirical thermal offset current $I_{off}(T)$, that is $I_{th}(T) = I_{tho} + I_{off}(T)$. The temperature-dependent offset current could be a function of any form, but for simplicity, it is taken as a polynomial function of temperature

$$I_{off}(T) = a_0 + a_1T + a_2T^2 + a_3T^3 + a_4T^4 + \dots \quad (2)$$

where the coefficient $a_0 - a_4$ can be determined during parameter extraction. It is important to note that because Eqn. 2 is not exclusively an increasing function of temperature, it should be able to capture the general temperature dependence of the VCSEL's LI curves.

Now that we have described a method to consider the thermal effect on the leakage current, we need an expression of the temperature characteristics of the VCSEL. While it is possible to adopt a numerical representation of a VCSEL's temperature profile as a function of the heat dissipation the device, a better method and more suitable for circuit level simulations is to describe the active region temperature via a thermal rate equation as follows [23]:

$$T = T_o + (IV - P_o)R_{th} - \tau_{th} \frac{dT}{dt} \quad (3)$$

where T_o is the ambient temperature, V is the terminal voltage of the laser, R_{th} is the VCSEL's thermal impedance which relates temperature change to the heat power dissipation, and τ_{th} is the thermal time constant which accounts to the nonzero response time of the device temperature (observed to be on the order of $1 \mu s$ [23]). Eqn. 3 also captures the thermal dynamics which is important in the transient characteristics of a VCSEL.

Rate Equations

As discussed before, the model should be able to simulate both static (DC) and dynamic (transient) modulation of the VCSEL. To do this, the model should be based on the laser rate equations. Fortunately, the simple above-threshold LI curves described by $P_o = \eta(I - I_{th})$ can be described by the standard laser rate equations [26]. Thus, by introducing the empirical offset current $I_{off}(T)$ into these equations, the model should be able to simulate the LI curves of the VCSEL at different temperature as well as the dynamic behavior such as small-signal and transient modulation.

After the addition of the offset current, the laser rate equations become:

$$\frac{dN}{dt} = \frac{\eta_i(I - I_{off}(T))}{q} - \frac{N}{\tau_n} - \frac{G_o(N - N_o)S}{1 + \varepsilon S} \quad (4)$$

$$\frac{dS}{dt} = -\frac{S}{\tau_p} + \frac{\beta N}{\tau_n} + \frac{G_o(N - N_o)S}{1 + \epsilon S} \quad (5)$$

where S is the photon number, N is the carrier number, N_o is the carrier transparency number, η_i is the injection efficiency, τ_n is the carrier recombination lifetime, G_o is the gain coefficient, τ_p is the photon lifetime, and β is the spontaneous emission coupling coefficient. As we can see, the introduction of the offset current into the rate equations is quite simple, however, it is an extremely effective means of describing the thermal dependence of the VCSEL's continuous wave LI characteristics. In addition, since the model is based on the rate equations, it should be able to simulate the non-dc behavior of the VCSEL. Finally, the optical output power is described using $P_o = kS$, where k is a scaling factor accounting for the output coupling efficiency of the laser.

Current/Voltage characteristics

The current-voltage relationship of the VCSEL can be expressed in great detail based on its diode-like characteristics, however, the voltage across the device in this model has been selected to be an arbitrary empirical function of current and temperature as follows:

$$V = f(I, T). \quad (6)$$

Then, the complete electrical characteristics of the VCSEL can be accounted for by introducing capacitors and other parasitics components in parallel with this voltage (in which case Eqn. 3 should be modified such that it depends on the total device current and not just I). The advantage of this approach is that since different VCSELs have different IV characteristics, the specific form of Eqn. 6 can be determined on a device-by-device basis. For example, the IV relationship could be modeled as $V = IR_s + V_T \ln(1 + I/I_s)$ where R_s is a series resistance, I_s is the diode's saturation current, and V_T is the diode's thermal voltage which is usually temperature dependent. In other cases, a polynomial function of current and temperature [23] such as

$$V = (b_0 + b_1T + b_2T^2 + \dots)(c_0 + c_1I + c_2I^2 + \dots) \quad (7)$$

can be used, where b_n and c_n are constant parameters to be extracted. It is important to note that if experimental IV data is used to determine all the other parameters of the model first, then the exact form of Eqn. 6 can be determined at the very end of parameter extraction of a specific device. This approach actually has many advantages. First, it allows the voltage's current and temperature dependence to be accurately modeled. Second, it permits the optical and electrical characteristics to be decoupled from one another, therefore simplifying the extraction of the model's parameters. For the VCSEL in consideration, the author provides only the IV characteristics at room temperature. That is why the IV data was fitted simply to a polynomial function of current as follows:

$$\begin{aligned} V = & 1.721 + 275I - 2.439 \times 10^4 I^2 + 1.338 \times 10^6 I^3 \\ & - 4.154 \times 10^7 I^4 + 6.683 \times 10^8 I^5 - 4.296 \times 10^9 I^6. \end{aligned} \quad (8)$$

Implementation

The large-signal model of the VCSEL follows from the rate equations, Eqn. 4 and Eqn. 5, from the temperature dependent offset current $I_{\text{off}}(T)$, from the thermal rate equation, Eqn. 3, and from the current/voltage characteristics of the diode described in Sec. . However, the implementation of the above equations as they are will lead to convergence problems and this is why variable transformation was used and the rate equations were normalized. First, S is transformed into a new variable X_s via $S = X_s/k$, and N into X_n via $N = z_n X_n$, where k is the output coupling efficiency and z_n is an arbitrary constants in the order of

10^7 . This will ensure that the state variables (X_s and X_n as discussed in the next section) will not take on very large values. Second, the rate equations were normalized so that every term in those equations is well behaved. That is, Eqn. 3 is divided by R_{th} , Eqn. 4 is multiplied by q/η_i and Eqn. 5 is multiplied by $\tau_p k$. The resulting equations are as follows:

$$\frac{T}{R_{th}} = \frac{T_o}{R_{th}} + (IV - P_o) - \frac{\tau_{th}}{R_{th}} \frac{dT}{dt} \quad (9)$$

$$\frac{qzn}{\eta_i} \frac{dX_n}{dt} = (I - I_{off}(T)) - \frac{qznX_n}{\eta_i \tau_n} - \frac{q}{\eta_i k} \frac{G_o(znX_n - N_o)X_s}{1 + \frac{\varepsilon}{k} X_s} \quad (10)$$

$$\tau_p \frac{dX_s}{dt} = -X_s + \frac{k\tau_p \beta znX_n}{\tau_n} + \frac{\tau_p G_o(znX_n - N_o)X_s}{1 + \frac{\varepsilon}{k} X_s} \quad (11)$$

Also, the model was modified to include the output wavelength λ which can be calculated from the carrier density N with the following equation [27]:

$$\lambda = \lambda_o [1 - \frac{\rho}{n}(N - N_o)] \quad (12)$$

where λ_o is the intrinsic band gap wavelength, ρ is the total variation of the refractive index due to the differences in injected current levels, and n is the refractive index of the medium.

To implement the model, we start by identifying the state variables, then by writing the model equations as a function of those state variables and their derivatives. Since the terminal voltage V is expressed in Eqn. 8 as a function of the current I (which could be the input terminal current or not depending on whether a parasitic capacitor C_l is included or not), I is chosen as the first state variable. Then, if C_l is not included, V can be directly written as a function of I . On the other hand, if C_l is included, then the total input current is expressed as $I_{tot} = I + I_{Cl}$ where $I_{Cl} = C_l dV/dt$ and can be expressed as:

$$I_{Cl} = C_l(c_1 + 2c_2 I + 3c_3 I^2 + 4c_4 I^3 + 5c_5 I^4). \quad (13)$$

Second, the three rate equations, Eqn. 9, 10, and 11, need to be satisfied. This is done by first augmenting the model with three ports (three terminals with their respective local reference terminals), second by letting the above equations be equal to the current at each of the respective port, and finally forcing that current to zero by connecting an open circuit to that port. It is very much in the same way Eqn. ?? was satisfied as described in Sec. ??.

Finally, the voltage at the designated optical output power is described by $P_o = (v_m + \delta)$ where the current is meaningless. The same should also be done for implementing Eqn. 12.

Simulations and Results

The purpose of the following sections is to present some of the results of the VCSEL model implemented in fREEDA.

In Sec. , a DC analysis is performed on the implemented VCSEL model. Graphs of the IV and LI curves at different ambient temperature are shown and compared to the measurements. Also, plots of the carrier number, output wavelength, and active region temperature versus the input current are presented.

Sec. presents the results of the transient analysis. The model is driven by an input current pulse of finite rise and fall time. All the transient simulations are carried out at 20 °C ambient temperature. Graphs of the carrier number and active region temperature versus time are presented. Also, plots of the optical output power and wavelength chirp are shown.

In Sec. a Harmonic Balance simulation is performed on the implemented VCSEL model. First, the frequency response of the VCSEL for an input rf power of -8 dBm is presented. Second, plots of the large signal wavelength chirp for different bias current is presented. Finally, the power ratio of the second harmonic

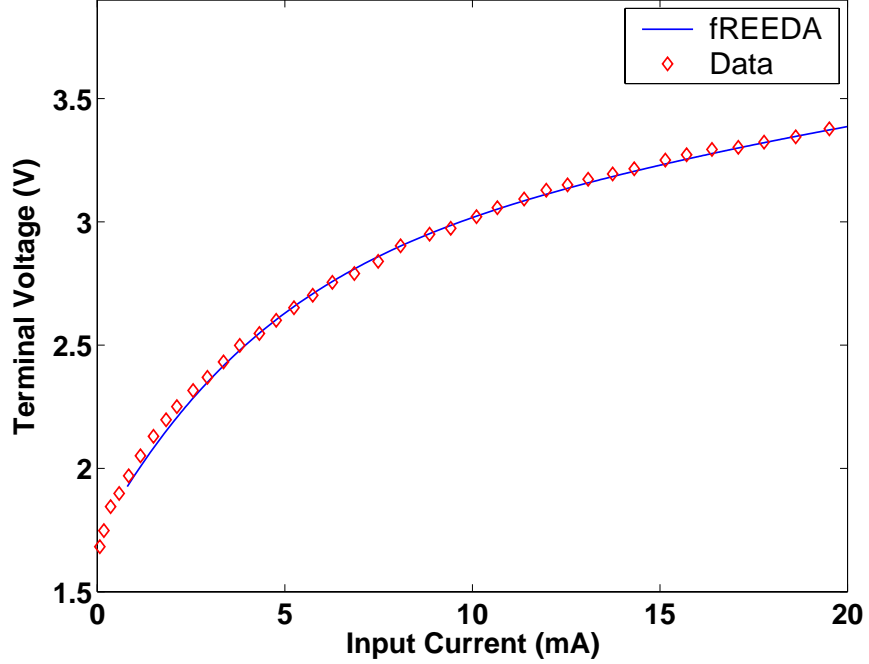


Figure 3: DC Analysis comparison of the IV curve of the VCSEL model and the measurement. Measurements from [23].

to the fundamental P_{2f}/P_f and of the intermodulation distortion to the fundamental P_{IM3}/P_f as a function of bias current and temperature are shown.

The fREEDA netlists which was used to generate the plots in the Reference [2].

DC Analysis

The input terminal current is varied from 0 mA to 37 mA and the simulation is run at 3 different ambient temperature, 20 °C, 60 °C, and 100 °C. Fig. 3 shows the IV curve of the VCSEL (only one curve is show since the IV characteristics of the diode is modeled as an independent function of temperature).

Plots in Fig. 4 shows a family of curves of the carrier number in the active region as a function of the input current at different ambient temperature. From this graph, we can clearly deduce two things. First, and as expected, the carrier number will not increase anymore once threshold is reached. Second, carrier leakage starts at a much lower input current at high ambient temperature. Also, as seen in Fig. 5, the wavelength is constant above threshold. This is due to the fact that the output wavelength is mainly a function of the carrier number. Finally, Fig. 6 shows the plots of the active region temperature versus the input current for different ambient temperature. It is clear from these plots how severely the VCSEL can be heated.

The optical output power as a function of the input current is shown in Fig. 7. From these plots, we can deduce a lot of things. First, there is a threshold current shift at different ambient temperatures. In addition, there is a significant reduction in the slope efficiency and the maximum output power. Finally, the effect of carrier leakage is obvious and manifest itself clearly in the optical output roll over and the complete turn-off of the laser.

As we can see in the IV and LI plots, there is an excellent agreement between the simulations in fREEDA and the measurements.

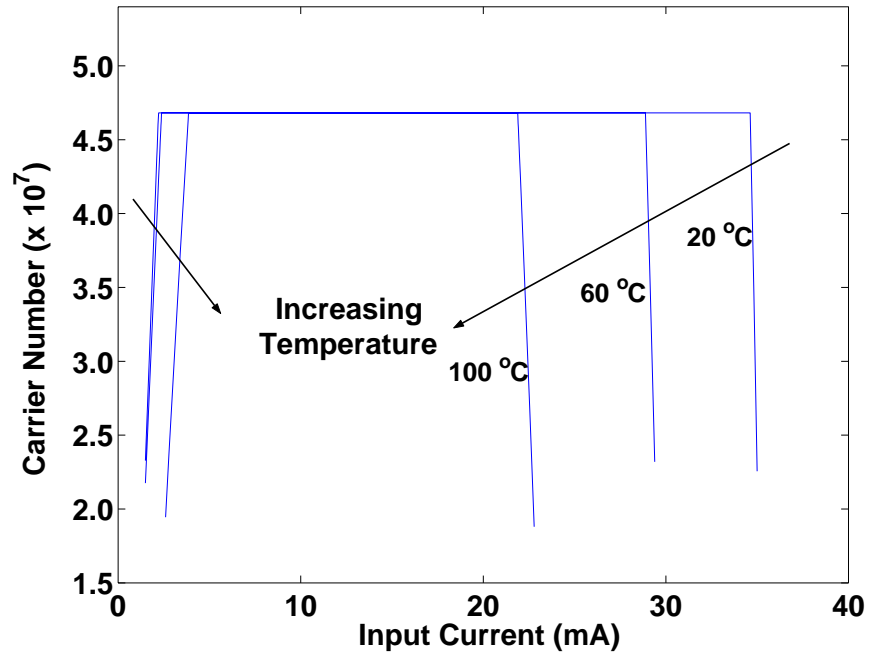


Figure 4: DC Analysis plots of the carrier number at different ambient temperature.

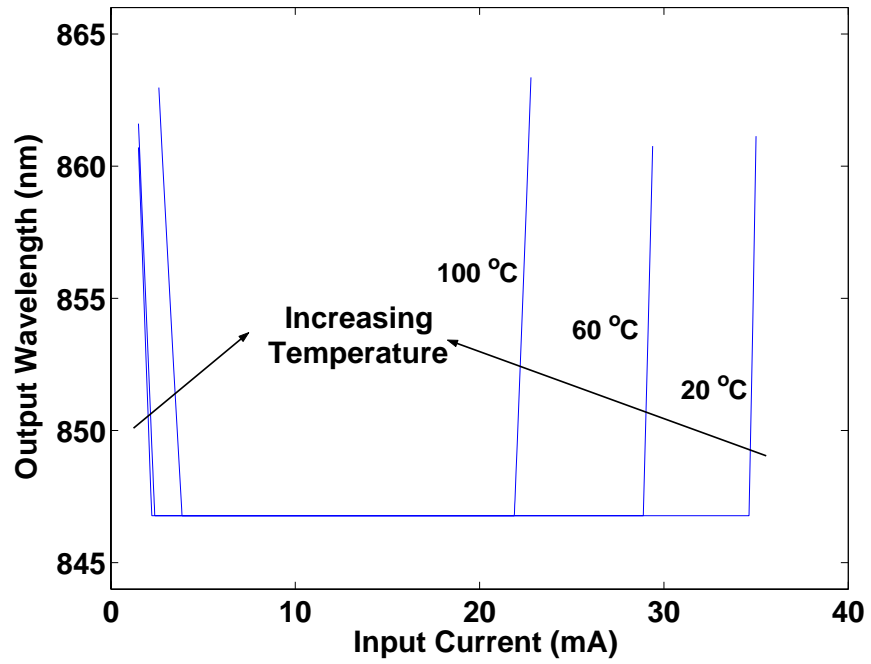


Figure 5: DC Analysis plots of the output wavelength at different ambient temperature.

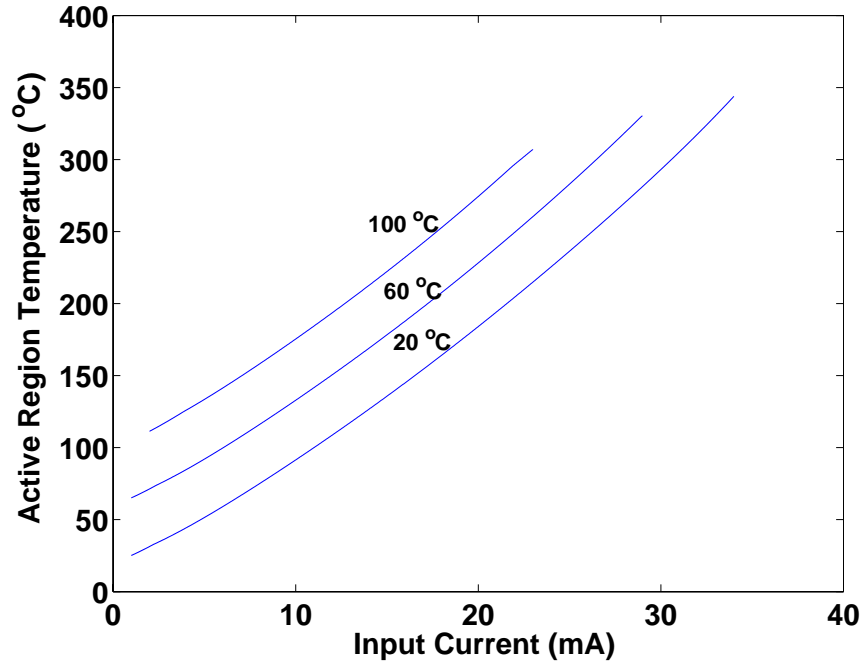


Figure 6: DC Analysis plots of the active region temperature increase at different ambient temperature.

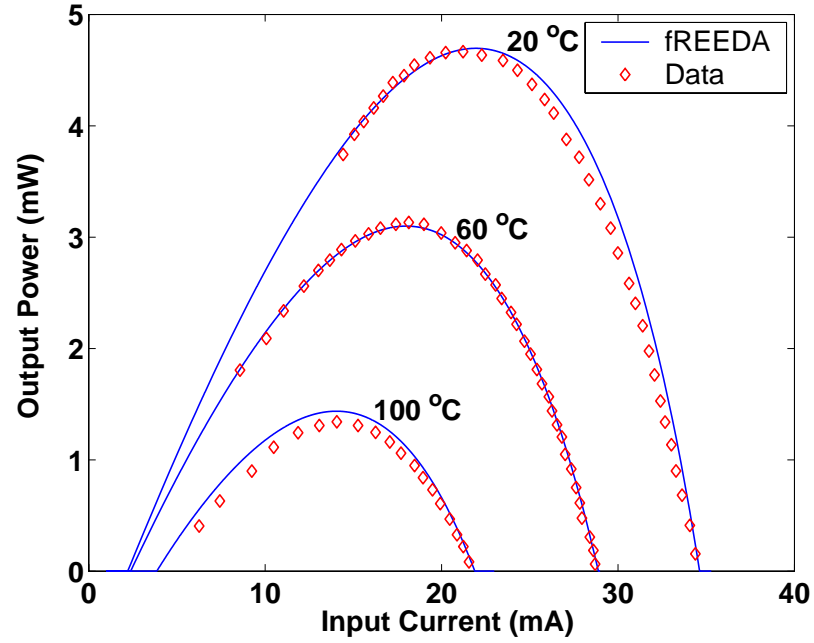


Figure 7: DC Analysis comparison of the *LI* curves at different ambient temperature with the measurement. Measurements from [23].

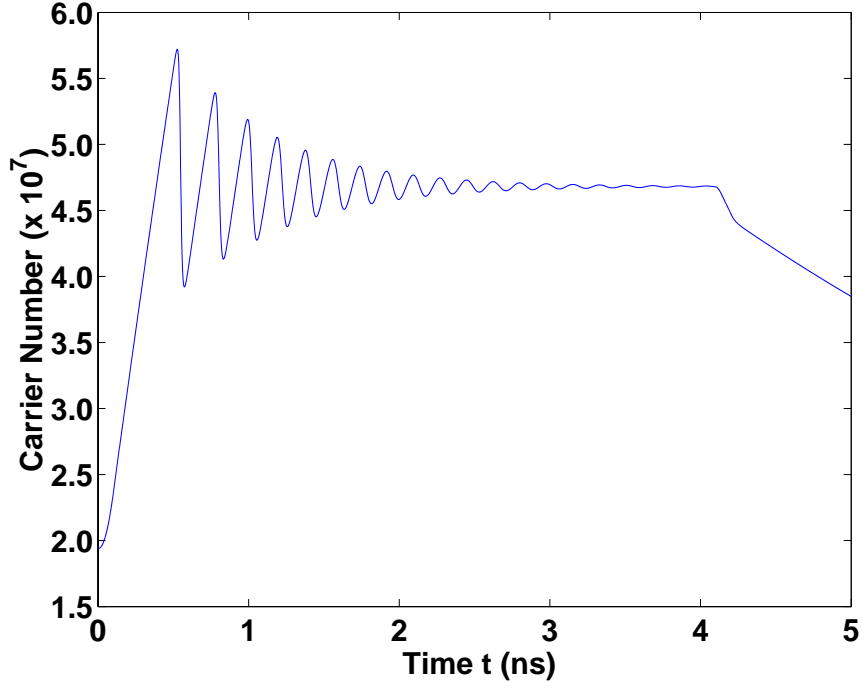


Figure 8: Transient analysis plot of the carrier number at 20 °C.

Transient Analysis

While DC simulations are very important to identify key factors such as threshold current, maximum output power and temperature effects in the VCSEL, transient analysis is also a crucial part in the design of OEICs. This is the main reason why the model was based on the laser rate equations.

The VCSEL is driven by a current pulse that has a peak value of 15 mA, a period of 5 nano-seconds, and a rise and fall time of 0.1 ns. The ambient temperature is set to 20 °C during the simulations. The plots in Fig. 8 show the carrier number versus time while Fig. 9 shows the plots of wavelength chirp which is a critical factor in the design of Wavelength Division Multiplexed (WDM) Systems. Fig. 10 shows how fast is the increase in the active region temperature and plots in Fig. 11 shows the optical output power. In the last figure, the optical output power shows the well known laser turn-on delay and ringing effects.

Harmonic Balance

VCSEL diodes are promising light sources for low-cost, high-performance optical microwave links in microcellular networks and high speed phased-array radar antenna [29]. Lately, analog fiber-optic link based on directly modulated VCSELs was also proposed to get rid of the digital data transmission limitations in hazardous highly radioactive environment with large temperature variation from 50 to 200 °C such as thermonuclear reactors [30]. It is therefore of great importance to characterize the VCSEL's behavior for analog applications at microwave frequencies.

In this section, Harmonic Balance was used to study the VCSEL's characteristics of importance to microwave modulation such as the modulation response, the large signal wavelength chirp, and most importantly the VCSEL's linearity as a function of bias current and ambient temperature. First, the laser was connected to the parasitic network shown in Fig. 12 and the VCSEL's harmonic response was characterized.

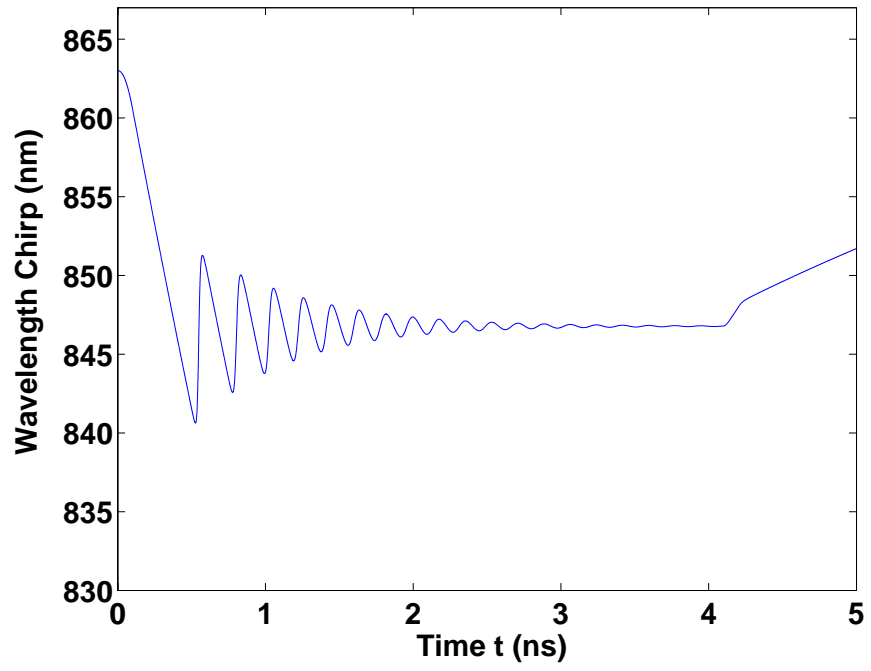


Figure 9: Transient analysis plot of the wavelength chirp at 20 °C.

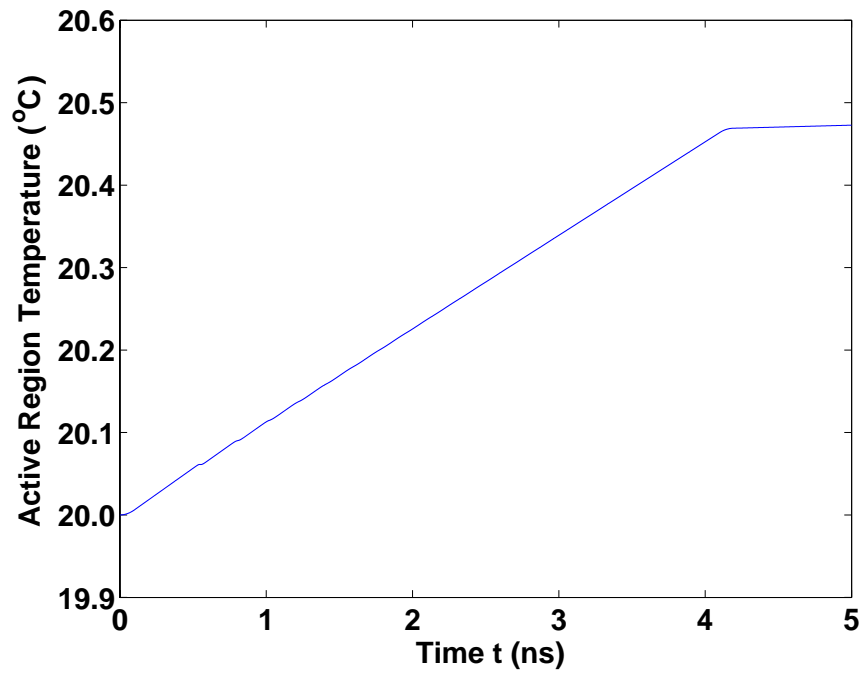


Figure 10: Transient analysis plot of the increase in the active region temperature at 20 °C.

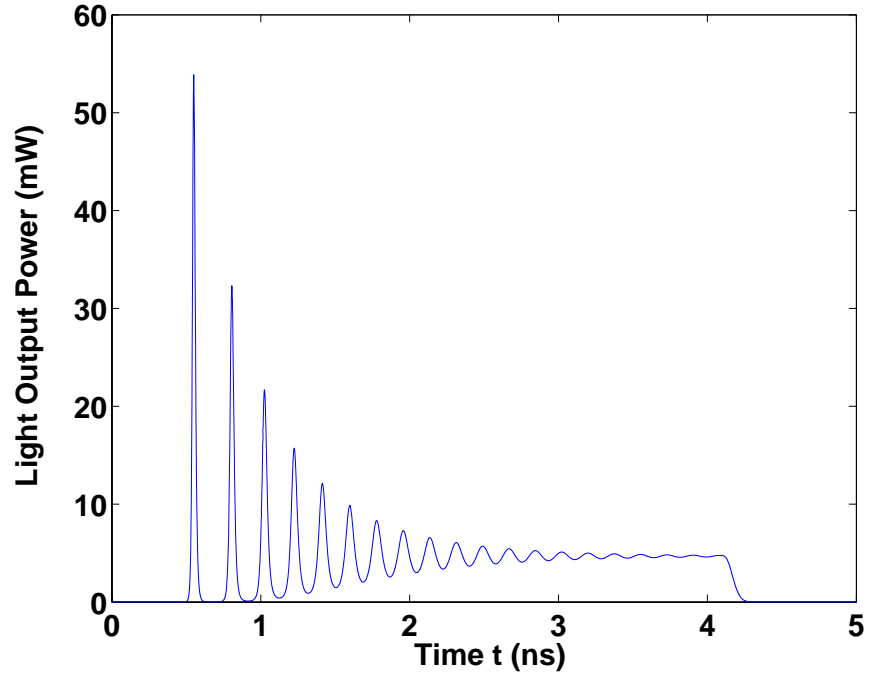


Figure 11: Transient analysis plot of the output optical power at 20 °C.

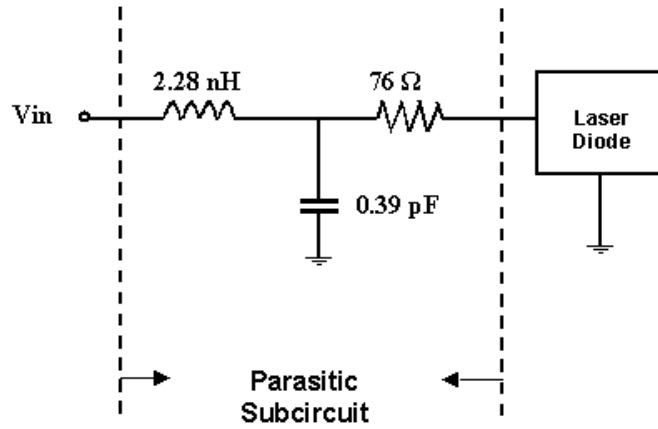


Figure 12: Parasitic network used in HB simulation. After [28].

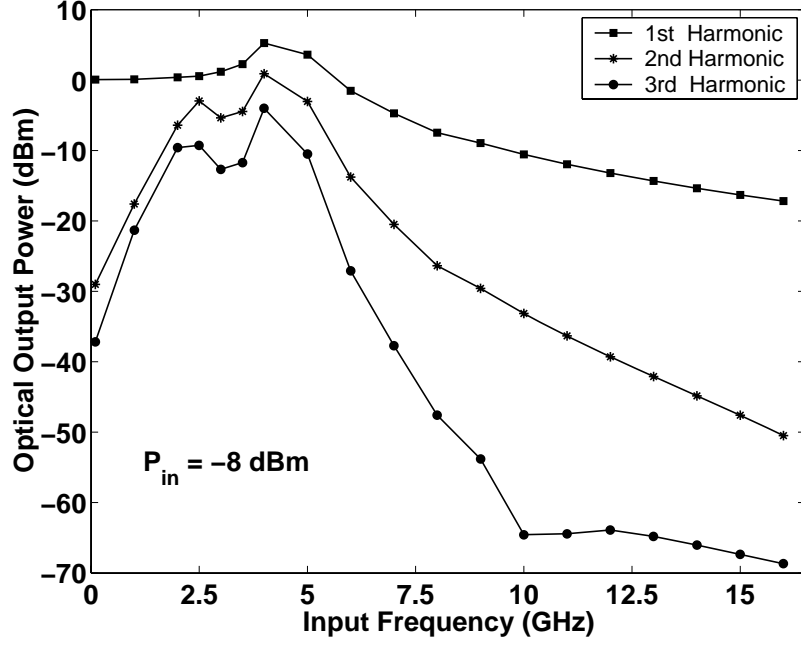


Figure 13: Frequency response of the first three harmonics for a constant input signal power of -8 dBm at 12 mA bias current.

The laser was driven by a single tone rf-input power of -8 dBm and the amplitude of the first three harmonic peaks were monitored as the signal frequency was varied. Fig. 13 shows the modulation response of the VCSEL at a bias current of 12 mA while Fig. 14 and 15 are the plots at a bias current of 14 mA and 16 mA respectively. As we can see, the first-order relaxation resonance frequency appears to be around 4 GHz and shifts towards 5 GHz at higher bias current. Also, the laser appears extremely nonlinear at this high input power specifically around the resonant frequency.

Fig. 16 shows the large signal wavelength chirp as the input frequency was varied at different bias current. The plots shows that the wavelength chirp increases with increasing bias current and it peaks at the resonant frequency.

Second, the VCSEL was driven by a single tone RF-input signal of -20 dBm at 1 GHz. Fig. 17 shows plots of the power ratio of the second harmonic to the fundamental P_{2f}/P_f as a function of bias current at different ambient temperature. The results shows that there is an increase in linearity with bias current up to the power rollover point where linearity starts to decrease again. It is also interesting to see this linearity level given the nonlinear LI curves of the laser (Fig. 7) and that the VCSEL is mostly linear around the maximum output power bias point. However, the VCSEL's linearity decreases considerably with increasing ambient temperature and this could be explained by the fact that at higher ambient temperature, the same input RF power will drive the VCSEL more into the off region leading to more harmonic distortion.

Finally, the VCSEL was driven by two signals of equal input power of -20 dBm at 1.0 GHz and 1.01 GHz. Fig. 18 shows the power ratio of the third-order intermodulation product to the carrier P_{IM3}/P_f as a function of the bias current at different ambient temperature. Again, the results shows that the VCSEL's nonlinear behavior is similar to the results described in the previous figure.

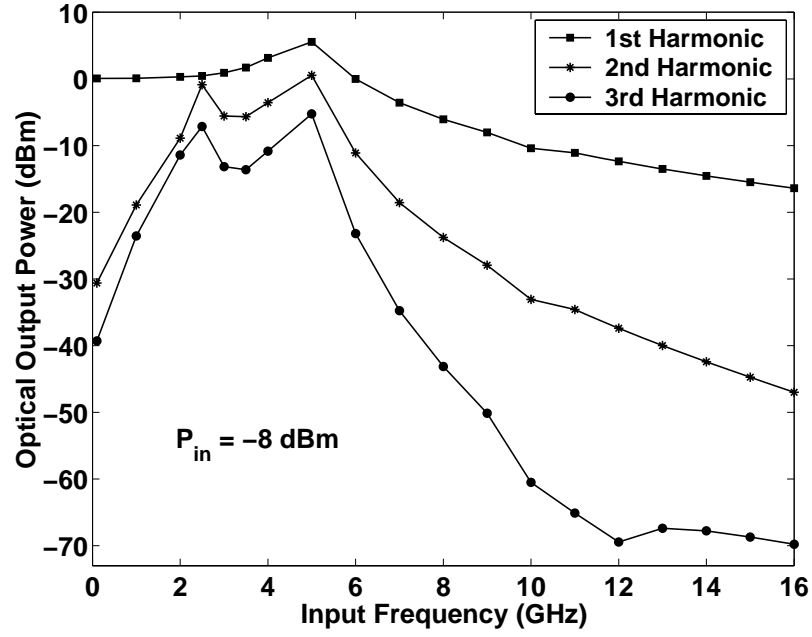


Figure 14: Frequency response of the first three harmonics for a constant input signal power of -8 dBm at 14 mA bias current.

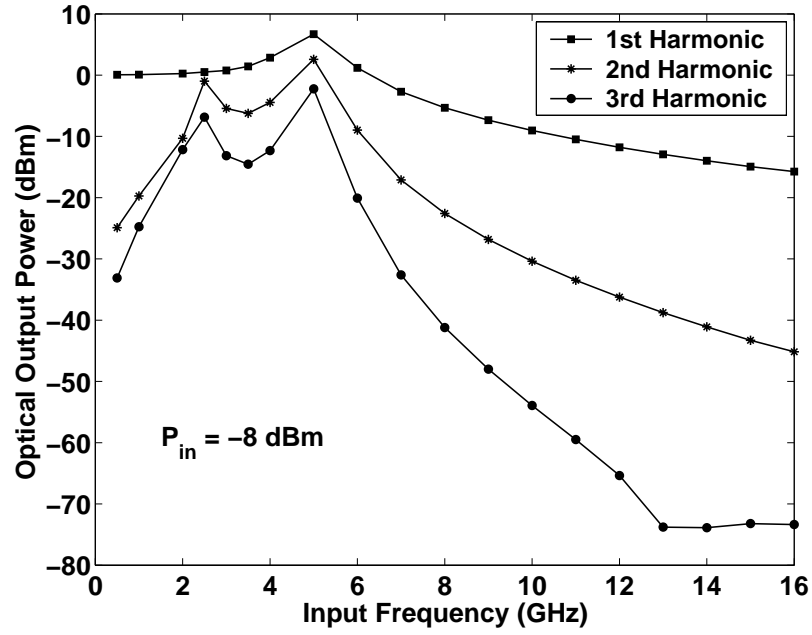


Figure 15: Frequency response of the first three harmonics for a constant input signal power of -8 dBm at 16 mA bias current.

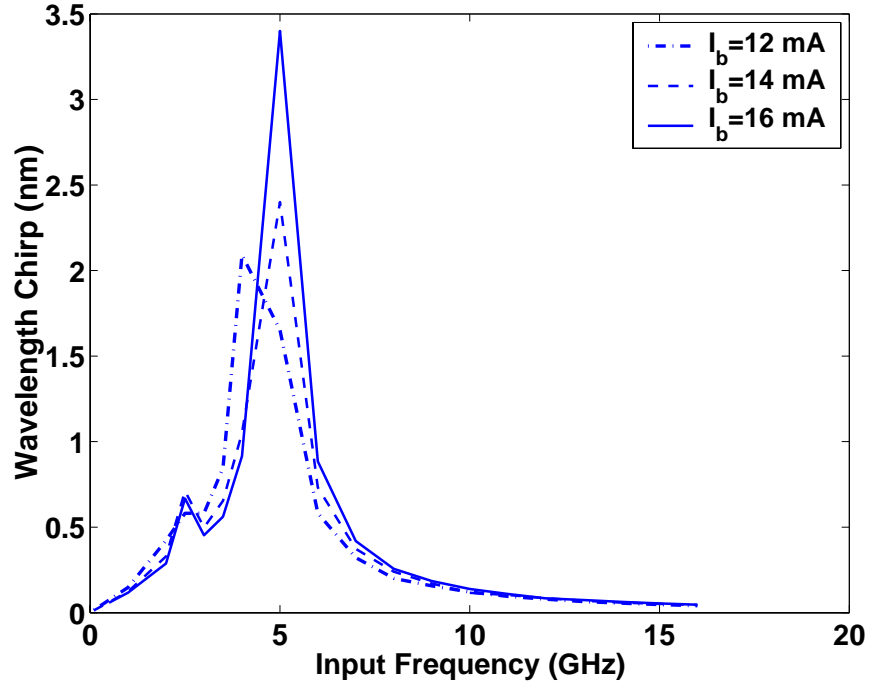


Figure 16: Plots of the wavelength chirp versus frequency at different bias current.

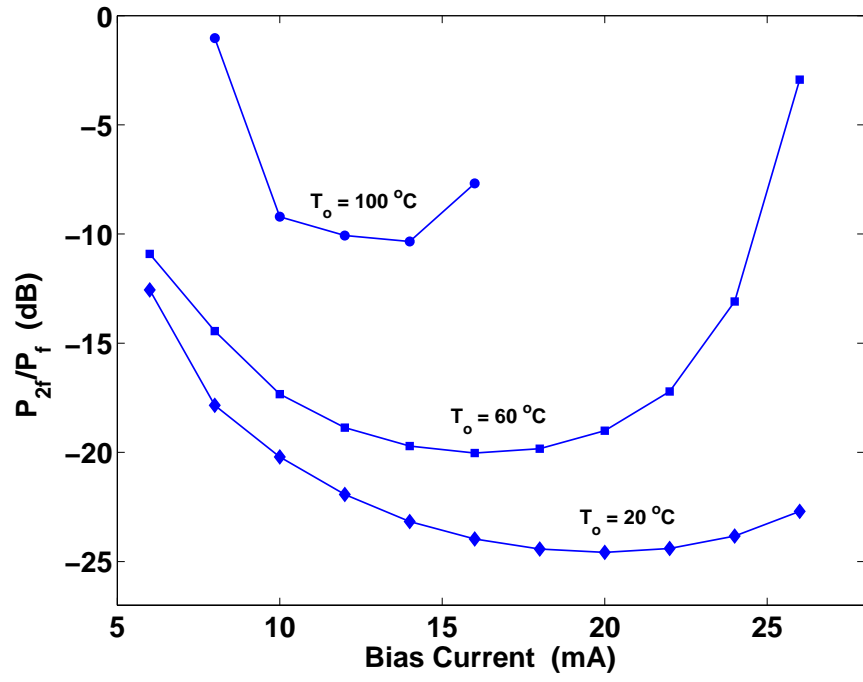


Figure 17: Power ratio of second harmonic to fundamental as a function of bias current for different temperature.

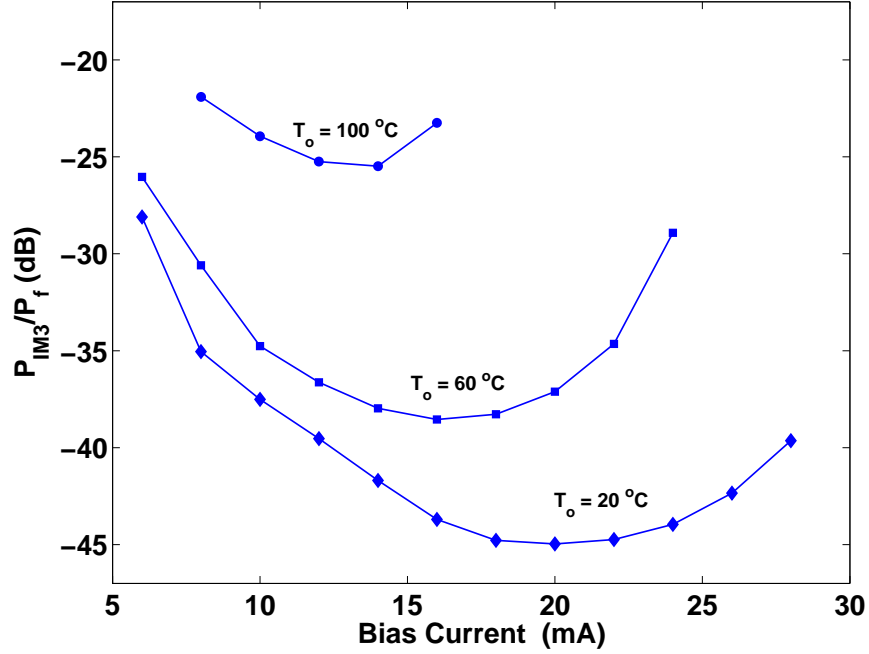


Figure 18: Power ratio of third-order intermodulation products to carrier as a function of bias current for different temperature.

References

- [1] R. Pant, M. A. Neifeld, M. B. Steer, H. Kanj, and A. C. Cangellaris, "Electrical package impact on VCSEL-based optical interconnects," *Optics Communication*, Vol. 245, Issue 1-6, Jan. 2005, p. 315-332.
- [2] H. Kanj, *Circuit-Level Modeling of Laser Diodes*, M.S., North Carolina State University, 2003.
- [3] N. Bewtra, D. A. Suda, G. L. Tan, F. Chatenoud, and J. M. Xu, "Modeling of Quantum-Well Lasers with Electro-Opto-Thermal Interaction," *IEEE J. of Selected Topics in Quantum Electronics*, Vol. 1, No. 2, pp. 331-340, June 1995.
- [4] J. Morikuni, G. Dare, P. Mena, A. Harton, K. Wyatt, "Simulation of optical interconnect devices, circuits, and systems using analog behavioral modeling tools," *IEEE Lasers and Electro-Optics Society Annual Meeting*, Vol. 1, pp. 235-236, Dec 1998.
- [5] <http://www.freda.org>.
- [6] A. Griewank, D. Juedes and J. Utke, "Adol-C: A Package for the Automatic Differentiation of Algorithms Written in C/C++," *ACM TOMS*, Vol. 22(2), pp. 131-167, June 1996.
- [7] J. Hecht, "Laser Pioneers" *Boston: Academic Press*, 1992.
- [8] R. D. Dupuis, "An Introduction to the Development of the Semiconductor Laser," *IEEE J. of Quantum Electronics*, Vol. QE-23, No. 6, June 1987.
- [9] J. Morikuni, P. Mena, A. Harton, K. Wyatt, "Optoelectronic Computer-Aided Design," *IEEE Lasers and Electro-Optics Society Summer Topical Meetings*, pp. 53-54, July 1998.
- [10] L. Seung-Woo, C. Eun-Chang, C. Woo-Young, "Optical interconnection system analysis using SPICE," *The Pacific Rim Conference on Lasers and Electro-Optics*, Vol. 2, pp. 391-392, Sep 1999.

- [11] C. E. Christoffersen, *Global Modeling of Nonlinear Microwave Circuits*, Ph.D. Dissertation, Dept. of Electrical Engineering, North Carolina State University, 2001.
- [12] W. B. Joyce, R. W. Dixon, "Electrical characterization of heterostructure lasers," in *J. Appl. Phys.*, Vol. 49, No. 7, July 1978.
- [13] R. S. Tucker, "Circuit model of double-heterojunction laser below threshold," in *IEE Proc. on Solid-State & Electron Devices-Part I*, Vol. 128, No. 3, pp. 101–106, 1981.
- [14] R. S. Tucker, "Large-signal circuit model for simulation of injection-laser modulation dynamics," in *IEE Proc. on Solid-State & Electron Devices-Part I*, Vol. 128, No. 5, pp. 180–184, 1981.
- [15] H.C. Casey, M.B. Panish, "Heterostructure Lasers, part A and part B" *Academic Press*, 1978.
- [16] L.A. Coldren, S.W. Corzine, "Diode Lasers and Photonic Integrated Circuits," *John Wiley & Sons, Inc.*, 1995.
- [17] V. Rizzoli, A. Lipparini, A. Costanzo, F. Matri, C. Cecchetti, A. Neri, D. Masotti, "State-of-the-art harmonic-balance simulation of forced nonlinear microwave circuits by the piecewise technique," *IEEE Transactions on Microwave Theory and Techniques*, Vol. 40, issue 1, pp. 12–28, Jan. 1992.
- [18] S. N. Velu, *Charge Based Modeling in State Variable Based Simulator*, M.S. Thesis, Dept. of Electrical Engineering, North Carolina State University, 2002.
- [19] W. I. Way, "Large Signal Nonlinear Distortion Prediction for a Single-Mode Laser Diode Under Microwave Intensity Modulation," *IEEE J. of Lightwave Technology*, Vol. LT-5, No. 3, March 1987.
- [20] S. Iezekiel, C. M. Snowden, "Nonlinear Circuit Analysis of Laser Diodes Under Microwave Direct Modulation," *IEEE MTT-S International*, Vol. 2, pp. 937–940, 1990.
- [21] E. Towe, R. F. Leheny, A. Yang, "A Historical Perspective of the Development of the Vertical-Cavity Surface-Emitting Laser," *IEEE J. on Selected Topics in Quantum Electronics*, Vol. 6, No. 6, Nov/Dec 2000.
- [22] Y. Ohiso, K. Tateno, Y. Kohama, A. Wakatsuki, H. Tsunetsugu, and T. Kurokawa, "Flip-chip bonded 0.85- μm bottom-emitting vertical-cavity laser array on an AlGaAs substrate," *IEEE Photon. Technol. Lett.*, Vol. 8, pp. 1115–1117, Sep 1996.
- [23] P. V. Mena, J. J. Morikuni, S.-M. Kang, A. V. Harton, K. W. Wyatt, "A Simple Rate-Equation-Based Thermal VCSEL Model," *IEEE J. of Lightwave Technology*, Vol. 17, No. 5, May 1999.
- [24] M. A. Neifeld (private communication), 2003.
- [25] G. Hasnain, K. Tai, L. Yang, Y. H. Wang, R. J. Fisher, J. D. Wynn, B. Weir, N. K. Dutta, and A. Y. Cho, "Performance of Gain-guided Surface Emitting Lasers with Semiconductor Distributed Bragg Reflectors," *IEEE J. of Quantum Electron.*, Vol. 27, No. 6, pp. 1377–1385, 1991.
- [26] G. P. Agrawal, and N. K. Dutta, "Semiconductor Laser, 2nd ed." *New York: Van Nostrand Reinhold*, 1995.
- [27] M. A. Neifeld and W. C. Chou, "Electrical packaging impact on source components in optical interconnect," *IEEE Transactions on Components, Packaging, and Manufacturing Technology — Part B*, Vol. 18, pp. 578–595, Aug. 1995.
- [28] M. Bruensteiner, G. C. Papen, "Extraction of VCSEL Rate-Equation Parameters for Low-Bias System Simulation," *IEEE J. of Selected Topics in Quantum Electron.*, Vol. 5, No. 3, 1999.

- [29] C. Carlsson, H. Martinsson, R. Schatz, J. Halonen, A. Larsson “Analog Modulation Properties of Oxide Confined VCSELs at Microwave Frequencies,” *IEEE J. of Lightwave Technology*, Vol. 20, No. 9, September 2002.
- [30] A. F. Fernandez, F. Berghmans, B. Brichard, M. Decreton, “Toward The Developement of Radiation-Tolerant Instrumentation Data Links for Thermonuclear Fusion Experiments,” *IEEE Transactin on Nuclear Science*, Vol. 49, No. 6, December 2002.


Known Bugs:

Several aspects of the model are hard coded for a specific case. The model needs to be generalized.

Version:

2003.01.01

Credits:

Name	Affiliation	Date	Logo
Houssam Kanj www.ncsu.edu	NC State University	2003	
Michael Steer www4.ncsu.edu/ mbs	NC State University	2003	